



Controlling the morphology of polybutadiene–poly(ethylene oxide) diblock copolymers in bulk and the orientation in thin films by attachment of alkyl side chains

A. Levent Demirel^{a,b,*}, Helmut Schlaad^b

^a Koç University, Chemistry Department, Sariyer 34450, Istanbul, Turkey

^b Max Planck Institute of Colloids and Interfaces, Colloid Department, Research Campus Golm, 14424 Potsdam, Germany

ARTICLE INFO

Article history:

Received 18 April 2008

Received in revised form 27 May 2008

Accepted 27 May 2008

Available online 4 June 2008

Keywords:

Semicrystalline–amorphous block

copolymers

Side chain effects

Morphology

ABSTRACT

A polybutadiene₁₉-block-poly(ethylene oxide)₉₄ (PB-PEO) has been modified by free-radical additions of 2-ethylhexanethiol, 1-decanethiol, and 1-dodecanethiol separately to the PB block. The block copolymers were characterized by DSC, SAXS, XRD and AFM measurements. Above the melting temperature of PEO, PB-PEO showed hexagonal morphology having PB cylinders in the PEO matrix. The addition of alkyl side chains decreased the volume fraction of PEO and the morphology changed to lamellar for ethylhexyl side chains and to reversed hexagonal morphology with PEO cylinders in the PB/alkyl chain matrix for decyl and dodecyl side chains. Below the melting temperature of PEO, all polymers showed lamellar morphology. In the case of dodecyl side chains, the lamellar morphology oriented perpendicular to the air/film interface and was stable against high temperature annealing.

© 2008 Elsevier Ltd. All rights reserved.

1. Introduction

Current research activities on block copolymer morphology focus, among other objectives, on increasing the length scales above the tens of nanometers, achieving long-range ordered morphologies and determining the orientation of the ordered structures. The self-organized morphology of block copolymers can successfully be controlled by varying the total degree of polymerization, N , the Flory–Huggins interaction parameter, χ , and the volume fraction, f , of the components. For conformationally isotropic AB diblock copolymers in the strong segregation limit where $\chi_{AB}N \gg 10$, the morphology changes from disordered to BCC spheres to hexagonal cylinders to lamellar as volume fraction of one component, say f_A , increases from 0 to 0.5 (f_B changes from 1 to 0.5). The morphology changes symmetrically on the other side of the phase diagram when f_A goes from 0.5 to 1 (f_B goes from 0.5 to 0). For a given pair of strongly incompatible components A and B, one way to change the morphology is to increase the degree of polymerization of one block, N_A , while keeping that of the other block, N_B , constant. For components having equal monomer volumes, going from $f_A = 0.25$ ($N_A = n$, $N_B = 3n$; hexagonal morphology) to

$f_A = 0.50$ ($N_A = 3n$, $N_B = 3n$; lamellar morphology) require increasing N_A by $2n$. An easier way of changing the composition is the attachment of side chains to the backbone of one component. To go from $f_A = 0.25$ to $f_A = 0.50$, the additional $2n$ monomers must be distributed between the starting $N_A = n$ backbone monomers. This is equivalent to attaching two monomer long side chains to each backbone monomer assuming 100% functionalization. In controlling the morphology, the synthetic route of attaching smaller side chains is much easier than increasing the degree of polymerization of one block due to high viscosities of large molecular weight components. In addition to the change of composition, the attachment of side chains also affects the morphology indirectly by changing the interaction parameter χ_{AB} .

The effect of side chain modifications on the morphology of the block copolymers has been previously investigated in various systems. In a polystyrene-*block*-poly(4-vinyl pyridine) (PS-PVP) copolymer, the detachment of the hydrogen-bonded pentadecylphenol side chains from PVP at high temperatures changed the lamellar morphology to hexagonal where PVP block formed cylinders in the mixture of PS-pentadecylphenol [1]. The increase in the side chain lengths usually stabilizes the structures. In layered mesophases of PS-*b*-fluorocarbon side chains attached PS (or PI), the degree of order of the mesophase increased with the length of the side chains [2]. A counterintuitive case was reported for polystyrene-*block*-poly((ethylene glycol)_x methacrylate)s as a function of side chain length. The order in the lamellar phase decreased with

* Corresponding author. Koç University, Chemistry Department, Sariyer 34450, Istanbul, Turkey. Fax: +90 212 3381559.

E-mail address: ldemirel@ku.edu.tr (A.L. Demirel).

2.4. Small-angle X-ray scattering

Scattering curves were recorded with a Kratky camera with slit collimation and a rotating anode instrument with pinhole collimation. Measurements with the Kratky camera were performed at 70 °C under vacuum using a proportional counter (Anton Paar, Graz, Austria). Scattering data were recorded in the range of $s = (2/\lambda)\sin\theta = 0.03\text{--}0.95\text{ nm}^{-1}$ (2θ scattering angle, $\lambda = 0.15418\text{ nm}$). For the pinhole system, a Nonius rotating anode (4 kW, Cu $K\alpha$) and an image-plate detector system were used. With the image plates placed at a distance of 40 cm from the sample, a scattering vector range from 0.05 nm^{-1} to 1.6 nm^{-1} was available. Two dimensional diffraction patterns were transformed into a 1D radial average of the scattering intensity.

2.5. Wide-angle X-ray diffraction

Powder WAXD measurements were done in reflection mode by Nonius diffractometer (Inel, France) using Cu $K\alpha$ radiation ($\lambda = 0.15418\text{ nm}$) and a position sensitive detector. The same samples were used for SAXS and XRD measurements.

2.6. Scanning force microscopy

SFM measurements were performed with a Nanoscope Multi-mode IIIa microscope (Digital Instruments, Santa Barbara, CA, USA) using silicon cantilevers having $k = 42\text{ N/m}$ (Nanoworld,

Switzerland). Surfaces were scanned at room temperature in tapping mode at a resonance frequency of 200–300 kHz.

3. Results and discussion

3.1. Thermal characterization

The melting and crystallization of PEO blocks were determined by DSC measurements. Fig. 1a shows the heating/cooling DSC scans of PB–PEO taken between 0 °C and +70 °C (thermal decomposition of the sample at higher temperatures, as indicated by less intense and shifted melting and crystallization peaks in subsequent cycles) and of modified PB–PEO block copolymers taken between –50 °C and +300 °C. After the first heating, the subsequent DSC cycles for the copolymers were reproducible without any significant shifts. The melting point of PEO was slightly higher for block copolymers PB/C10–PEO and PB/C12–PEO containing linear C10 and C12 side chains ($T_m \sim +54.5\text{ °C}$) as compared to PB/C8–PEO containing branched C8 side chains ($T_m \sim +52.5\text{ °C}$). Also, PB/C12–PEO exhibited a slightly lower crystallization temperature ($T_c \sim +23.5\text{ °C}$) than PB/C10–PEO and PB/C8–PEO ($T_c \sim +25.5\text{ °C}$). For PB/C12–PEO only, side chain crystallization and melting were observed at –23.0 °C and –13.0 °C, respectively. The decrease in the side chain crystallization/melting temperatures with respect to the bulk value of –7.0 °C indicates confinement effects by the crystalline PEO lamellae [14].

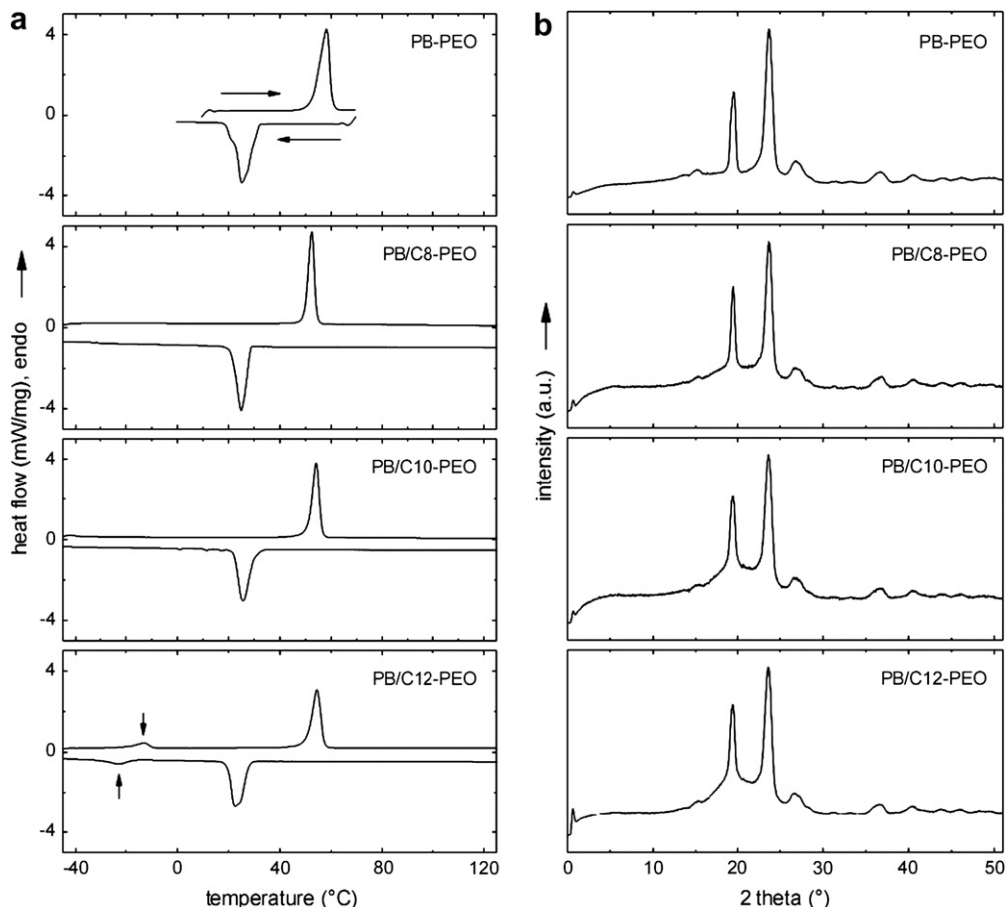


Fig. 1. (a) Second heating and cooling DSC scans for the block copolymers PB–PEO, PB/C8–PEO, PB/C10–PEO, and PB/C12–PEO (top to bottom). Arrows in the bottom panel indicate side chain crystallization and melting (PB/C12–PEO only). (b) Room temperature XRD data of the 70 °C annealed block polymers PB–PEO, PB/C8–PEO, PB/C10–PEO, and PB/C12–PEO (top to bottom).

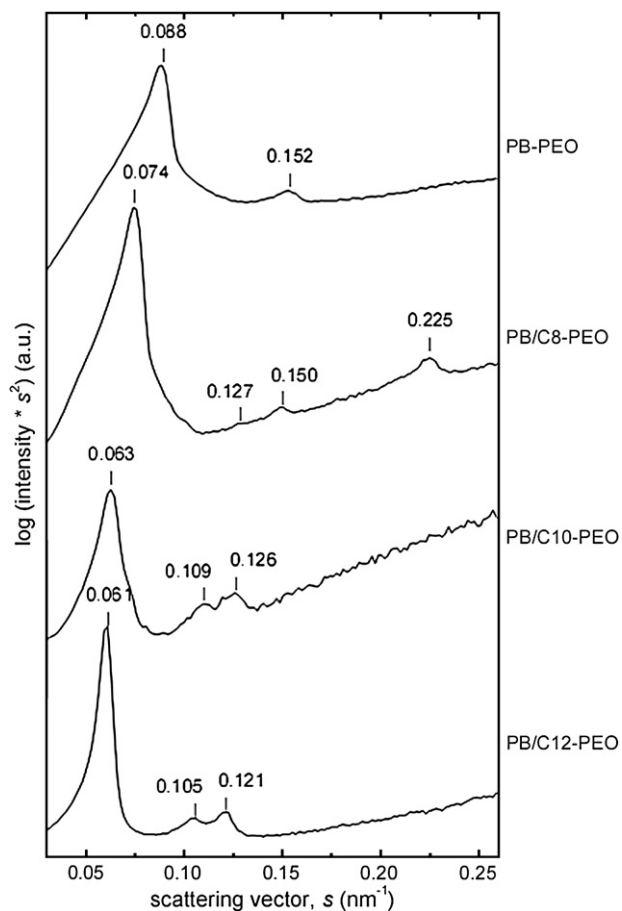


Fig. 2. SAXS curves (Kratky camera) measured for the films of block copolymers PB-PEO, PB/C8-PEO, PB/C10-PEO, and PB/C12-PEO (top to bottom) at 70 °C.

3.2. Structural characterization

The crystalline structure of the PEO did not show any difference for different side chains. Fig. 1b shows the XRD data of the polymers annealed at 70 °C and quenched to room temperature. For all samples, the two most intense peaks were observed at $2\theta = 19.5^\circ$ and 23.6° , respectively.

In the SAXS data (Fig. 2) recorded at 70 °C, that is above the melting temperature of PEO, the first-order reflection for the parent PB-PEO appeared at a scattering vector $s^* = 0.088 \text{ nm}^{-1}$,

corresponding to a Bragg spacing of $d = 11.4 \text{ nm}$. The additional scattering peak at $s = 0.152 \text{ nm}^{-1} = \sqrt{3}s^*$ indicates the presence of hexagonal morphology of cylinders, the distance between the cylinders, L , being 13.2 nm. Considering the calculated volume fractions ($f_{\text{PB}} = 0.25$ and $f_{\text{PEO}} = 0.75$, see Table 1), the hexagonal morphology consists of PB cylinders in a PEO matrix (Fig. 3a). A measured length of 6.6 nm for PB and PEO implies that both blocks are highly stretched compared to the radius of gyration (R_g). The value of R_g of the PB block is 0.51 nm and that of the PEO block is 1.4 nm. The contour lengths of blocks are 5.4 nm and 33.1 nm, respectively.

PB/C8-PEO, which has 2-ethylhexyl side chains attached to the PB block, adopted a lamellar (Fig. 3b) instead of a hexagonal morphology at 70 °C as confirmed by SAXS (Fig. 2). The first-order scattering peak is located at $s^* = 0.074 \text{ nm}^{-1}$ ($d = 13.5 \text{ nm}$) and higher-order lamellar peaks are seen at 0.150 nm^{-1} ($2s^*$) and 0.225 nm^{-1} ($3s^*$). A transition from hexagonal to lamellar morphology due to the side chain attachment is in agreement with the decrease of the PEO volume fraction from 0.75 in PB-PEO to 0.51 in PB/C8-PEO (Table 1). A very weak peak at $s = 0.127 \text{ nm}^{-1} = \sqrt{3}s^*$ ($L = 15.6 \text{ nm}$) may correspond to the presence of hexagonal perforated lamellae [10]. Assuming that the PEO block size is about $2R_g$, the upper limit for the length of PB/C8 block at 70 °C should be $\sim 4 \text{ nm}$. Stiffening of the PB backbone and a highly stretched PB/C8 block is expected due to the attached side chains. Because the attached alkyl side chains are above their melting temperatures, they should be randomly oriented around the PB backbone resulting in a “bottle-brush” structure. The attached 2-ethylhexyl side chains to $\sim 70\%$ of PB monomers thus hinder the bending of the PB backbone due to steric repulsion.

Polymers PB/C10-PEO and PB/C12-PEO showed hexagonal morphologies at 70 °C as shown in SAXS data of Fig. 2. For PB/C10-PEO, the first-order reflection appears at a scattering vector $s^* = 0.063 \text{ nm}^{-1}$, corresponding to a Bragg spacing of $d = 15.9 \text{ nm}$. The additional scattering peaks at $s = 0.109 \text{ nm}^{-1} = \sqrt{3}s^*$ and $s = 0.126 \text{ nm}^{-1} = 2s^*$ confirm the presence of the hexagonal morphology of PEO cylinders in the PB/C10 matrix (Fig. 3c). The distance L between the PEO cylinders is 18.4 nm. For PB/C12-PEO, the first-order reflection appears at a scattering vector $s^* = 0.061 \text{ nm}^{-1}$, corresponding to a Bragg spacing of $d = 16.4 \text{ nm}$. Similar to PB/C10-PEO SAXS data, additional scattering peaks were also observed for PB/C12-PEO at $s = 0.105 \text{ nm}^{-1} = \sqrt{3}s^*$ and $s = 0.121 \text{ nm}^{-1} = 2s^*$ indicating a hexagonal morphology of PEO cylinders in the PB/C12 matrix (Fig. 3c). The distance L between the PEO cylinders is 19.0 nm. Assuming fully stretched PB/C10 and PB/C12 blocks of length 5.4 nm, the radius of the PEO cylinders is calculated to be 3.8 nm and 4.1 nm, respectively.

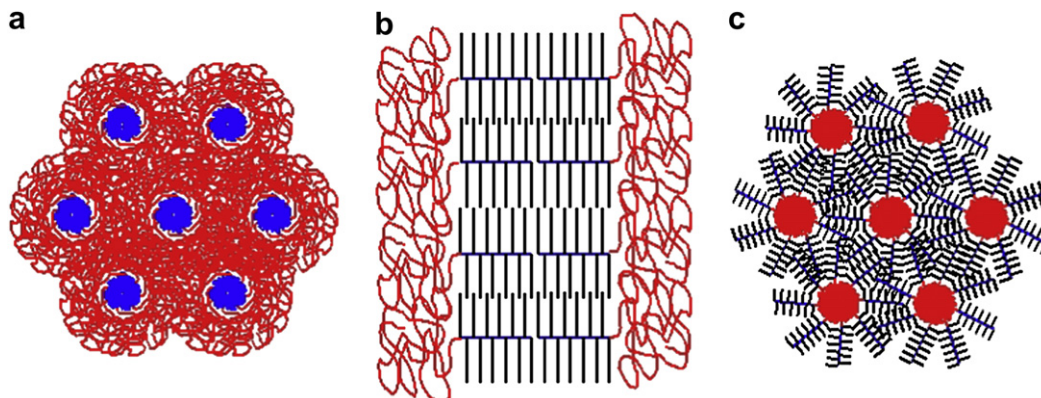


Fig. 3. Illustrations of morphologies observed. (a) PB-PEO: hexagonal morphology of PB cylinders in a PEO matrix. (b) PB/C8-PEO: lamellar morphology. (c) PB/C10-PEO, PB/C12-PEO: hexagonal morphology of PEO cylinders in a PB/C10 or PB/C12 matrix.

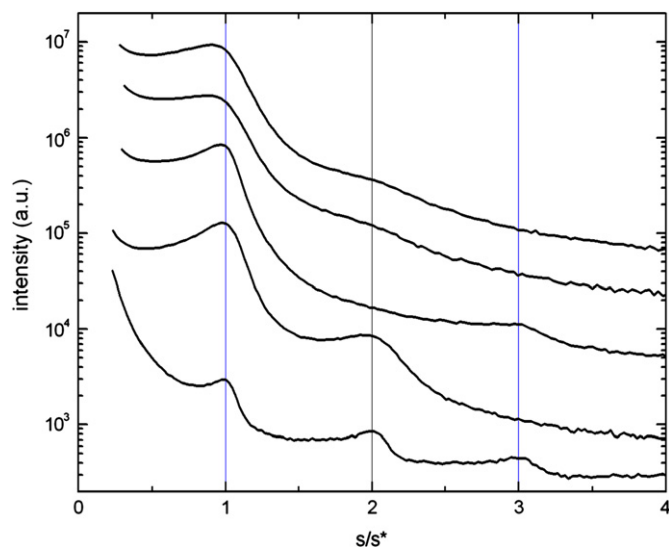


Fig. 4. SAXS data taken at room temperature after 70 °C annealing and quenching to room temperature. From bottom to top: PEO homopolymer, PB-PEO, PB/C8-PEO, PB/C10-PEO, PB/C12-PEO.

Below the melting point of PEO, all samples showed lamellar morphology with integer multiples of s/s^* in SAXS data (Fig. 4). The values of s^* (and d) were 0.072 nm^{-1} (13.8 nm) for PB-PEO, 0.057 nm^{-1} (17.3 nm) for PB/C8-PEO, 0.054 nm^{-1} (18.4 nm) for PB/C10-PEO and PB/C12-PEO.

For PB/C8-PEO, the intensity of the second-order scattering peak is much weaker compared to third order scattering peak. This can be explained by the extinction rule of structural symmetry due to nearly equal layer thicknesses for both the PEO and the PB/C8 lamellae. PEO chains should be folded three or seven times, depending on whether they form interdigitated or bilayered lamellae. Both possibilities are consistent with the cross-sectional area that each block occupies at the interface. Fig. 5a shows the cross-sectional area of the PB/C8 block at the interface. At room temperature, the side chains are molten and orient randomly in all directions perpendicular to the backbone. The dark square at the center represents the PB backbone which is perpendicular to the plane. The segments emanating from the central square represent the side chains pointing randomly in all directions in the plane. For PB/C8, the side chain length corresponds to the length of six all-*trans* C–C bonds ($\sim 0.75 \text{ nm}$, see Chart 1); the cross-sectional area of the PB/C8 block is then about $1.5 \times 1.5 \text{ nm}^2$. Fig. 5b shows the cross-sectional area of the PEO crystal structure in the fold-plane

[15]. The lines connecting the filled squares represent the chain folds in the plane. The chain axis bends down at filled squares. The dashed line represents the chain folds at the bottom fold-plane. The cut view of the polymer chain along the dashed line is seen in Fig. 5c. An area of $1.3 \times 1.3 \text{ nm}^2$ consists of total of seven folds, four are seen in the top fold-plane and the three in the bottom fold-plane.

For C10 and C12 side chains, a long period of 18.4 nm was measured at room temperature without any indication of structural symmetry. Considering a PB length between 4.3 nm (measured for PB/C8) and 5.4 nm (fully stretched), the PEO thickness should be 7.6–9.8 nm. In the case of bilayers of folded PEO, chains should be folded 6–7 times similar to that observed for PB/C8-PEO. For the parent PB-PEO block copolymer, a long period of 13.8 nm was measured at room temperature. Assuming that the PB block size is $\sim 2R_g$, the PEO fold length is calculated to be $\sim 5.9 \text{ nm}$, indicating that the PEO chains would be folded five times in a bilayer. The decrease in number of folds is consistent with the available cross-sectional area that PB block occupies at the interface. Under the same preparation and crystallization conditions, the PEO homopolymer exhibiting a contour length of 40 nm showed a first-order SAXS scattering peak at $s^* = 0.066 \text{ nm}^{-1}$ ($d = 15.2 \text{ nm}$) (bottom curve in Fig. 4), which corresponds to 1–2 folds.

The lamellar morphology formed by the polymers at room temperature could be confirmed by SFM measurements. Fig. 6 shows the SFM phase pictures of the polymers after spin-coating, after annealing at 70 °C for 2 h, and after annealing at 130 °C for 2 h. The corresponding SFM height pictures of the polymers annealed at 70 °C for 2 h are seen in Fig. 7. The PB-PEO sample showed indications of a lamellar morphology after spin-coating, which by annealing improved into ordered lamellae perpendicular to the substrate. The periodicity of the lamellae at room temperature was $\sim 15 \text{ nm}$ for both 70 °C and 130 °C annealed films, which is consistent with SAXS measurements. PB/C8-PEO also showed disordered regions of lamellar morphology after spin-coating. A perpendicular orientation of lamellar morphology could not be observed after annealing. The peak-to-peak surface roughness of $\sim 10\text{--}20 \text{ nm}$ in the height images (Fig. 7) supports parallel orientation of the lamellae with respect to the air/film interface.

Both PB/C10-PEO and PB/C12-PEO showed after spin-coating well-defined lamellar morphologies oriented perpendicular to the substrate. The period of the lamellar morphology in both cases was about 20 nm. PB/C10-PEO films just showed patches of perpendicular alignment after annealing suggesting a transition from perpendicular to parallel orientation of the lamellae. This was also supported by the observation of $\sim 20 \text{ nm}$ deep holes in the SFM

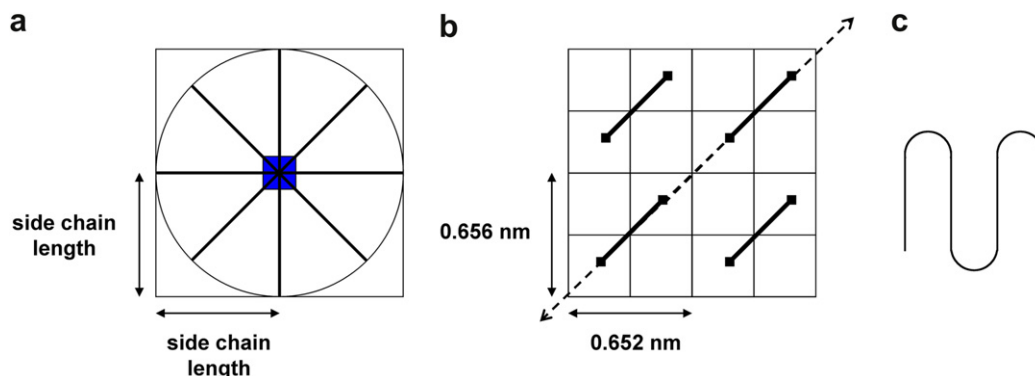


Fig. 5. (a) The cross-sectional area of the PB/C8 block at the interface. The dark square at the center represents the PB backbone which is perpendicular to the plane. The segments emanating from the central square represent the side chains pointing randomly in all directions in the plane. (b) The cross-sectional area of the PEO crystal structure in the fold-plane. The lines connecting the filled squares represent the chain folds in the plane. (c) The cut view of the polymer chain along the dashed line in (b).

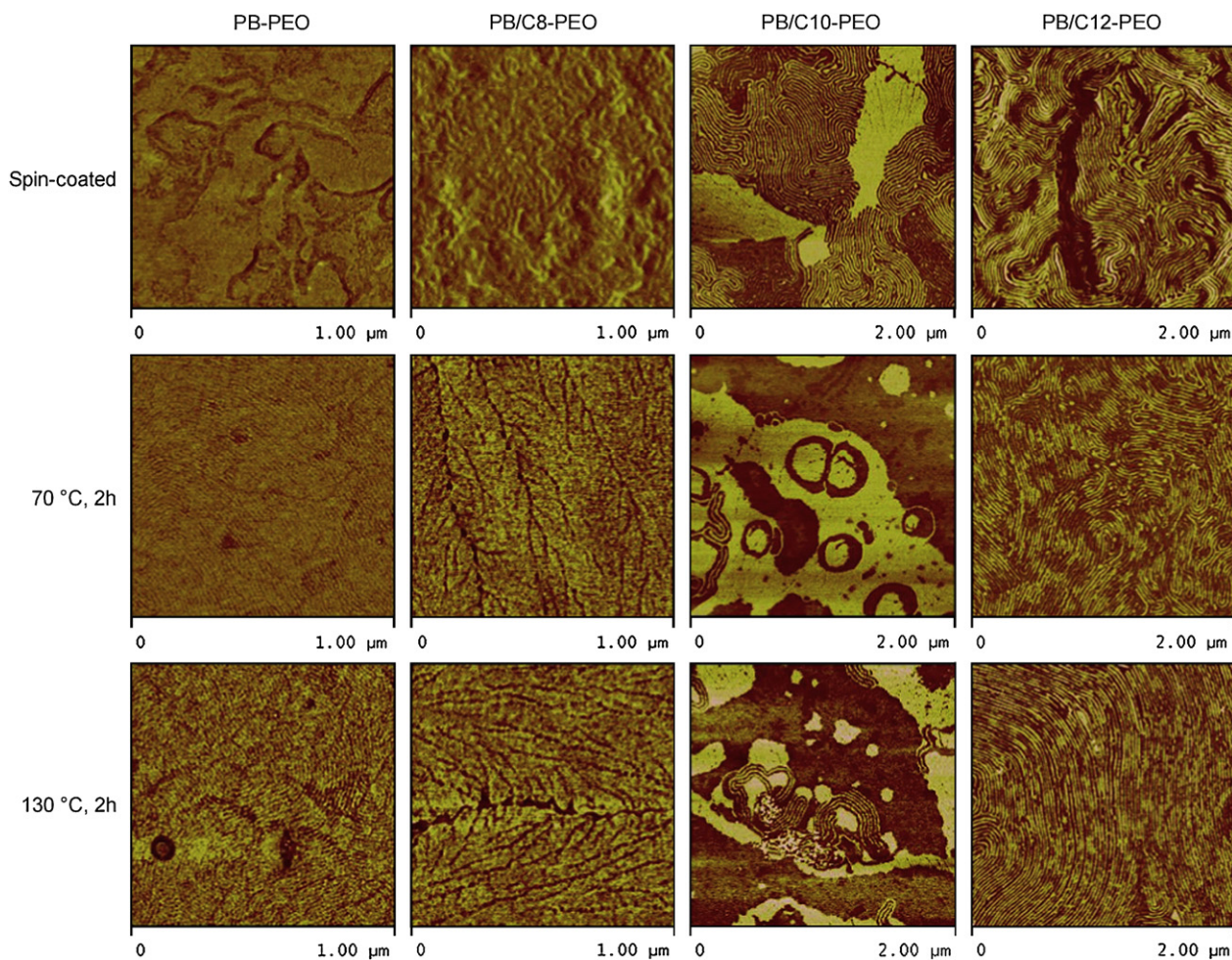


Fig. 6. SFM phase pictures of films of PB-PEO, PB/C8-PEO, PB/C10-PEO, PB/C12-PEO (left to right) after annealing at 70 °C for 2 h, and annealing at 130 °C for 2 h (top to bottom).

height picture (Fig. 7). In contrast, the perpendicularly oriented lamellar morphology of PB/C12-PEO films persisted after annealing with enhanced long-range order and smooth surface topography. The period of the lamellae stayed constant at ~ 20 nm. A transition in the orientation of the lamellae from parallel orientation to substrate above the melting temperature to perpendicular orientation by crystallization has previously been predicted [11]. This transition is induced kinetically by a decrease in the lamellar spacing for crystal growth rates larger than a critical value. In our case, it is not only the orientation but also the morphology that change by crystallization of PB/C10-PEO and PB/C12-PEO polymers. In isothermal crystallization experiments by DSC, crystallization was

slower for PB/C12-PEO compared to PB/C10-PEO and the observation of perpendicular lamellae cannot be attributed to any effect of crystallization rate. Based on the observation of parallel and perpendicular orientations for branched C8 side chains, mixed regions of parallel and perpendicular orientations for C10 side chains and perpendicular orientation for C12 side chains, we concluded that the longer alkyl side chains stabilize the perpendicular orientation of the lamellar morphology at the air/film interface of thin films due to the tendency of the methyl groups of the alkyl side chains to order at the air/film interface. A well-ordered methyl terminated surface at the air/film interface has previously been observed with a comb-shaped copolymer having alkyl side chains [16].

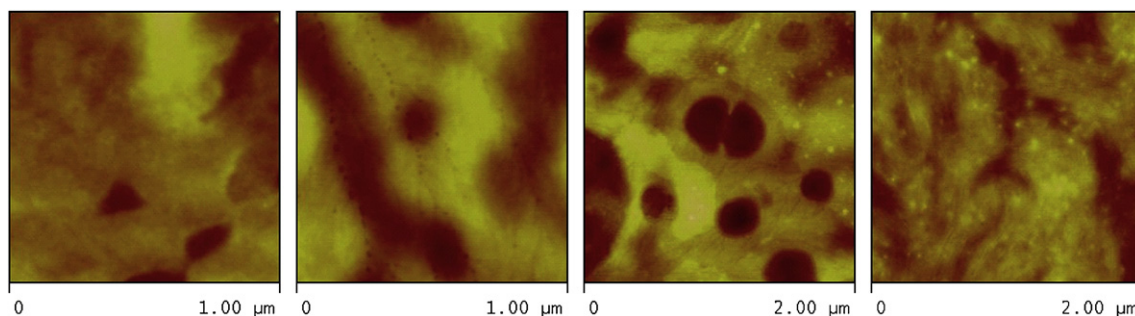


Fig. 7. SFM height pictures of films of PB-PEO, PB/C8-PEO, PB/C10-PEO, PB/C12-PEO (left to right) after annealing at 70 °C for 2 h.

4. Conclusions

A PB₁₉–PEO₉₄ diblock copolymer was grafted with three different alkyl side chains (C8: 2-ethylhexyl, C10: dodecyl, C12: dodecyl), and samples were characterized by DSC, SAXS, XRD and AFM. The attachment of alkyl side chains decreased the volume fraction of the PEO block and the morphology changed from hexagonal arrangement for PB–PEO (PB cylinders in PEO matrix), to a lamellar arrangement for PB/C8–PEO, and to an inverse hexagonal arrangement for PB/C10–PEO and PB/C12–PEO (PEO cylinders in PB/C10 or PB/C12 matrix) above the melting temperature of PEO. At room temperature, the structure formation was dominated by the crystallization of PEO and all polymers showed lamellar morphologies. In thin films, the orientation of the lamellae at the air/film interface changed from parallel to perpendicular with longer side chains due to the tendency of methyl groups to order. The perpendicular orientation of the PB/C12–PEO lamellae was stable after several hours of annealing at 130 °C. The results clearly show that the side chain attachment is a simple way to manipulate the composition (and thus the morphology) for the desired application. The alkylated PB–PEO system has the potential to achieve larger periodicities in microphase-separated structures due to stiffening of PB block by side chains and to control the orientation of the ordered structures in thin films. The stable perpendicular orientation of lamellae observed in this system allows the use of these structures as templates in nanolithographic applications.

Acknowledgments

We thank Ines Below for the synthesis of the block copolymers and the Max Planck Society for financial support.

References

- [1] Ruokolainen J, Mäkinen R, Torkkeli M, Mäkela T, Serimaa R, ten Brinke G, et al. *Science* 1998;280:557.
- [2] Andruzzi L, Chiellini E, Galli G, Li X, Kang SH, Ober CK. *J Mater Chem* 2002;12:1684.
- [3] Ishizone T, Han S, Hagiwara M, Yokoyama H. *Macromolecules* 2006;39:962.
- [4] Shenhar R, Sanyal A, Uzun O, Rotello VM. *Macromolecules* 2004;37:92.
- [5] Förster S, Berton B, Hentze HP, Krämer E, Antonietti M, Lindner P. *Macromolecules* 2001;34:4610.
- [6] Deng Y, Young RN, Ryan AJ, Fairclough JPA, Norman AI, Tack RD. *Polymer* 2002;43:7155.
- [7] Sommer JU, Reiter G. *Adv Polym Sci* 2006;200:1.
- [8] Nandan B, Hsu JY, Chen HL. *J Macromol Sci Part C Polym Rev* 2006;46:143.
- [9] Reiter G, Castelein G, Sommer JU, Röttele A, Thurn-Albrecht T. *Phys Rev Lett* 2001;87:226101.
- [10] Lambrev DM, Opitz R, Reiter G, Frederik PM, de Jeu WH. *Polymer* 2005;46:4868.
- [11] Reiter G, Castelein G, Hoerner P, Riess G, Blumen A, Sommer JU. *Phys Rev Lett* 1999;83:3844.
- [12] Semenov AN. *Macromolecules* 1993;26:6617.
- [13] Justynska J, Hordyjewicz Z, Schlaad H. *Polymer* 2005;46:12057.
- [14] Hempel E, Budde H, Höring S, Beiner M. *Thermochim Acta* 2005;432:254.
- [15] Takahashi Y, Tadokoro H. *Macromolecules* 1973;6:672.
- [16] Gautam KS, Dhinojwala A. *Macromolecules* 2001;34:1137.